Analyst

ROYAL SOCIETY OF CHEMISTRY

PAPER

View Article Online
View Journal | View Issue

Check for updates

Cite this: *Analyst*, 2023, **148**, 1349

A vertically paired electrode for redox cycling and its application to immunoassays†

Jun-Hee Park,[a] Ga-Yeon Lee,[a,b] Zhiquan Song,[a] Ji-Hong Bong,[a] Hong-Rae Kim,[a] Min-Jung Kang[c] and Jae-Chul Pyun*[a]

An electrochemical immunoassay based on the redox cycling method was presented using vertically paired electrodes (VPEs), which were fabricated using poly(3,4-ethylenedioxythiophene):poly(styrenesulfonate) (PEDOT:PSS) as an electrode material and parylene-C as a dielectric layer. For the application to immunoassays, different electrochemical properties of PEDOT:PSS were analyzed for the redox reaction of 3,3′,5,5′-tetramethylbenzidine (TMB, the chromogenic substrate for enzyme-immunoassays) at different pH conditions, including the conductivity (σ), electron transfer rate constant (k_{app}), and double-layer capacitance (C_{dl}). The influencing factors on the sensitivity of redox cycling based on VPE based on PEDOT:PSS were analyzed for the redox reaction of TMB, such as the electrode gap and number of electrode pairs. Computer simulation was also performed for the redox cycling results based on VPEs, which had limitations in fabrication, such as VPEs with an electrode gap of less than 100 nm and more than five electrode pairs. Finally, the redox cycling based on VPE was applied to the medical diagnosis of human hepatitis-C virus (hHCV) using a commercial ELISA kit. The sensitivity of the redox cycling method for the medical diagnosis of hHCV was compared with conventional assay methods, such as TMB-based chromogenic detection, luminol-based chemiluminescence assay, and a rapid test kit (lateral flow immunoassay).

Received 8th October 2022,
Accepted 12th February 2023

DOI: 10.1039/d2an01648f

rsc.li/analyst

Published on 21 febbraio 2023. Downloaded on 26/04/2026 03:20:33.

1. Introduction

Redox cycling is a modified amperometry method that amplifies the current signal through repeated oxidation and reduction of the target analytes.[1–6] Conventional single-mode amperometry is performed using a single working electrode (generator), and it generates a signal from the reduction (or oxidation) of analyte molecules. In the case of redox cycling, the analyte molecule is involved in the repeated oxidation and reduction cycle between two working electrodes called generator and collector electrodes. Therefore, the resulting signal is amplified through the repeated redox reactions (cycles) between the two working electrodes. The electrode gap must be as small as possible to maximize the efficiency of the redox cycling since the analyte is mass-transported between the generator and collector electrodes through diffusion.

The interdigitated electrode (IDE) is often used extensively for redox cycling, and the redox cycling was previously reported to be amplified up to 10-fold compared with conventional single-mode amperometric detection.[1,2,6,7] The first electrode (WE1, generator) was made up of one pair of IDE, as shown in Fig. 1(a), while the second electrode (WE2, collector) was made up of the other pair of IDE. The electrode gap needs to be fabricated as narrowly as possible in order to increase the efficiency of redox cycling because the electrode gaps affect the diffusion of the redox couple. This is because the efficiency of redox cycling sharply increases as the electrode gap between the two electrodes decreases. However, the electrode gap for IDE based on lab-based photolithography was limited to several micrometers.[1,2,8] Furthermore, costly processes such as e-beam lithography or stepper processes are required to fabricate the IDE under micrometers. In the previous report, we showed that the vertically paired electrode (VPE) could be easily fabricated as an electrode with a submicrometer electrode gap.[9,10] The electrode gap between each electrode was easily controlled to be less than one micrometer using parylene as a dielectric layer because the fabrication of VPE has been carried out by sequential deposition and etching process, and various metals (Au, Pt, and so on) have been used as electrode materials.[10] Recently, poly(3,4-ethylenedioxythiophene):poly(styrenesulfonate) (PEDOT:PSS) was reported to be

[a]*Department of Materials Science and Engineering, Yonsei University, 50 Yonsei-Ro, Seodaemun-Gu, Seoul 03722, Korea. E-mail: jcpyun@yonsei.ac.kr; Fax: +82 2 312 5375; Tel: +82 2 2123 5851*
[b]*Electronic Convergence Division, Korea Institute of Ceramic Engineering and Technology (KICET), Jinju, Korea*
[c]*Korea Institute of Science and Technology (KIST), Seoul, Korea*
† Electronic supplementary information (ESI) available. See DOI: https://doi.org/10.1039/d2an01648f

Published on 21 febbraio 2023. Downloaded on 26/04/2026 03:20:33.

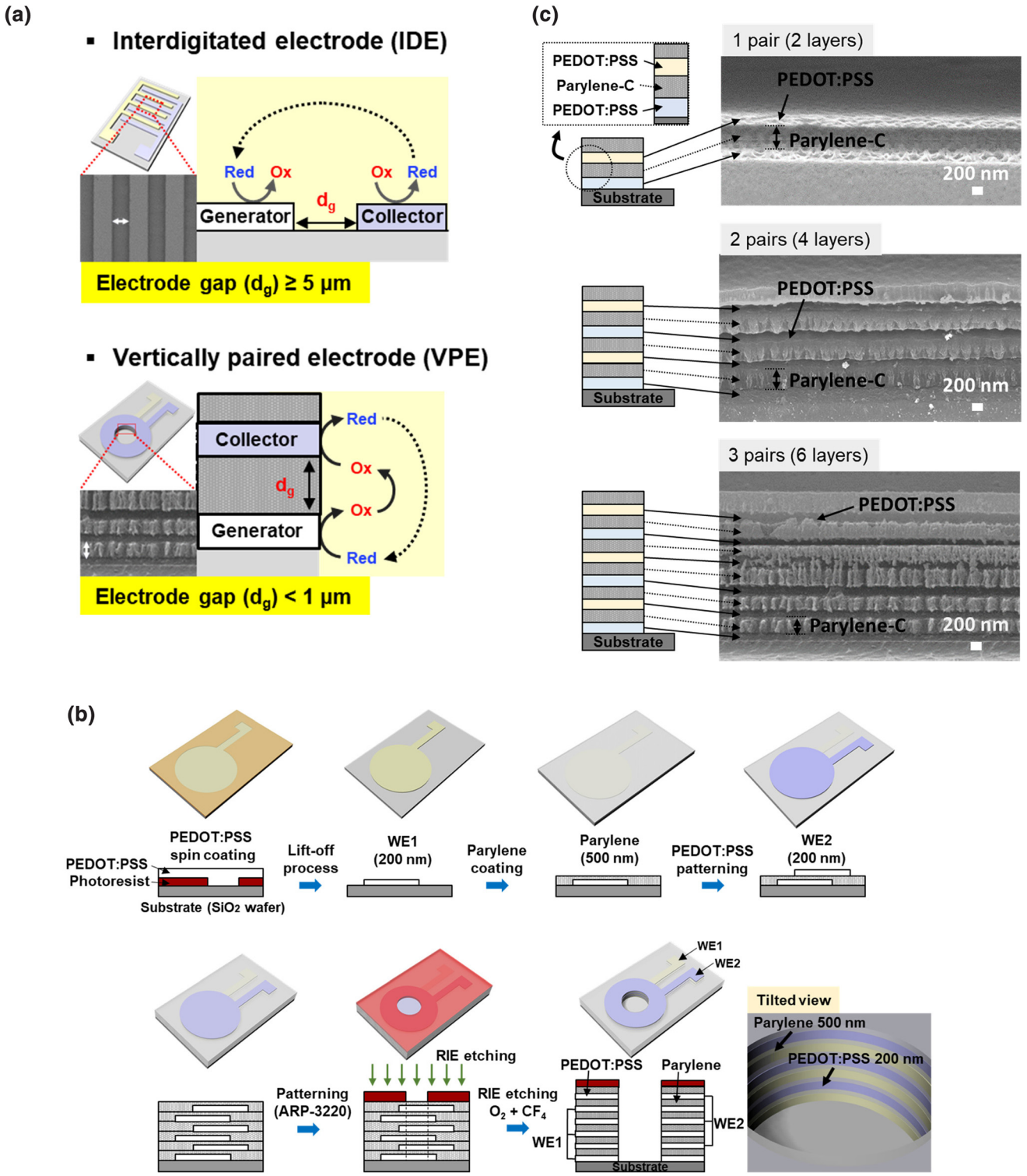

Fig. 1 Fabrication procedure of the vertically paired electrode (VPE). (a) Comparison of an interdigitated electrode (IDE) and vertically paired electrode (VPE). (b) Fabrication process of the vertically paired electrode. (c) SEM images of VPEs with different numbers of electrodes.

effectively used for the fabrication of VPE to increase the fabrication yield in comparison with metal electrodes by avoiding the electric shot problem from an incomplete wet-etching process.[11,12] Using PEDOT:PSS as an electrode material (200 nm) and parylene-C as a dielectric layer (500 nm), sequential deposition and etching processes were used to fabricate VPE, as shown in Fig. 1(b). The electrode was then exposed to reactive-ion etching (RIE), which could etch the electrode

This journal is © The Royal Society of Chemistry 2023

Published on 21 febbraio 2023. Downloaded on 26/04/2026 03:20:33.

material and the dielectric layer by a single step process. Therefore, the electrode gap of VPE could be made to be much shorter than the conventionally used IDE, and the so-made VPE was applied for the hypersensitive immunoassay through the electrochemical measurement of 3,3′,5,5′-tetramethybenzidine (TMB, the chromogenic substrate of enzyme-immunoassays).[13,14]

In this study, VPEs with a different number of electrode pairs were fabricated using PEDOT:PSS as an electrode material and parylene-C as a dielectric layer. The influencing factors for the sensitivity of VPE were analyzed according to the electrode gap and the number of electrode pairs using the redox reaction of TMB, and the computer-simulated results. Finally, a commercial ELISA kit was used to perform redox cycling detection based on the VPE for the medical diagnosis of human hepatitis-C virus (hHCV). The sensitivity of redox cycling was compared to the TMB-based chromogenic detection, luminol-based chemiluminescence assay, and a commercial rapid test (lateral flow immunoassay).[15–18]

2. Experimental section

2.1 Materials and methods

The conducting polymer PEDOT:PSS, TMB, and phosphate citrate buffer were purchased from Sigma-Aldrich Korea (Seoul, Korea). hHCV ELISA kits were bought from Innovation Biotech Co. (Beijing, China). hHCV rapid test (lateral flow immunoassay) was purchased from Abbott Korea (Seoul, Korea). Polystyrene microplates were bought from SPL Co. (Seoul, Korea). The photoresists (AZ-GXR601 and ARP-3220) were purchased from NM Tech (Namyangju, Korea). Ag/AgCl reference electrodes were purchased from Warner Instruments, LLC (Hamden, CT, USA). The counter electrodes were made from Pt wire with a diameter of 2 mm.

2.2 Fabrication of VPE

The VPE was fabricated on a SiO_2 wafer by sequentially depositing a PEDOT:PSS electrode (200 nm) and parylene-C film (500 nm), as shown in Fig. 1(b).[19,20] The wafer was cleaned with acetone and IPA before the photoresist (GXR601) was patterned on it. PEDOT:PSS electrodes were spin-coated on the photoresist (PR) and baked at 170 °C on the hot plate. Acetone was used to eliminate PR (lift-off process). A parylene-C film (500 nm) was deposited between the PEDOT:PSS electrodes by thermal deposition according to the following steps: (1) evaporation of parylene-C dimers at 180 °C, (2) pyrolysis of dimer into the monomer radical at 650 °C, and (3) deposition on the PEDOT:PSS electrode at room temperature.[21,22] The deposition process was repeated to fabricate 2-pair and 3-pair electrodes. The hole-structure with a 2 mm diameter was fabricated on the top-layer of VPE using photoresist (ARP-3220) on the parylene. Finally, the electrodes were exposed to the RIE process with a mixture of O_2 and CF_4 gas and 100 W power. The thickness of parylene-C and PEDOT:PSS was measured using AFM from Park Systems (Suwon, Korea).

2.3 Characterization of PEDOT:PSS electrode

The conductivity of PEDOT:PSS (thickness of 200 nm) was measured using the 4-point probe system (KEITHLEY 2400 source meter, USA). The conductivity was estimated according to the following equation: $\sigma = L/(R{\cdot}A)$, where L represents the distance between the 4 probes (1 mm), A represents the thickness of the film (200 nm), and R represents the measured resistance.[23]

The double-layer capacitance was estimated according to the equation: $i = C{\cdot}(\mathrm{d}V/\mathrm{d}t)$, where C represents the capacitance, and the capacitance corresponds to the linear slope of the current (i) at a given potential (0 V against Ag/AgCl) of series of magnitudes of the cyclic voltammogram at different scan rates, as shown in Fig. S1(a).† [24,25] The CV was performed using a commercial IVIUM potentiostat (Eindhoven, Netherlands). The Ag/AgCl pellet pseudo reference electrode (Warner Instrument LLC) was used as a reference electrode.

The k_{app} value represents the electron transfer rate constant for the redox reaction of the following equation: $\mathrm{d}[Fe(CN)_6^{4-}]/\mathrm{d}t = k_{app}{\cdot}[Fe(CN)_6^{3-}]$.[26] The k_{app} value for the PEDOT:PSS electrode was determined according to the Nicholson method, as shown in Fig. S1(b).† [27,28]

2.4 Redox cycling with VPE

The redox cycling was carried out as previously reported.[1,2] The redox cycling signal was measured using a bi-potentiostat from IVIUM potentiostat (Eindhoven, Netherlands). The Ag/AgCl pellet pseudo reference electrode (Warner Instrument LLC) was used as a reference electrode. When the stability of the Ag/AgCl pellet reference electrode was tested using the Ag/AgCl (3 M KCl) reference electrode from Metrohm (catalog #: 6.0733.100), the open circuit potential (OCP) between the two reference electrodes was within the error range (±5 mV) of the reference electrode at +2.397 mV.[29] The redox cycling signal was measured by changing the potential of the collector electrode while the cyclic voltammetry (CV) was performed at the generator electrode. As the first step, the potential of the collector electrode was controlled to be the reductive potential of −200 mV against the Ag/AgCl electrode while the generator electrode carried out CV of ox-TMB-2. The fixed potential of the collector electrode at −200 mV was used for the reduction of ox-TMB-2 (into TMB), which amplified the oxidative current of the cyclic voltammogram at the generator electrode (noted as "(1)" in Fig. 3(a)). As the second step, the potential of the collector electrode was controlled to be the oxidative potential of +400 mV against the Ag/AgCl electrode while the generator electrode carried out the CV of ox-TMB-2. The fixed potential of the collector electrode at +400 mV was used for the oxidation of TMB (into ox-TMB-2), which amplified the reductive current of the cyclic voltammogram at the generator electrode (noted as "(2)" in Fig. 3(a)). The final signal was calculated from the difference between the increased oxidative current of the first step (noted as "*" in Fig. 3(a)) and the increased reductive current at the second step (noted as "**" in Fig. 3(a)).

Published on 21 febbraio 2023. Downloaded on 26/04/2026 03:20:33.

2.5 Immunoassay for hHCV

The ELISA test for antibodies against the human hepatitis-C virus (hHCV) from Innovation Biotech Co. (Beijing, China) was performed according to the manufacturer's instructions.[30] From the manufacturer's instruction, the commercial ELISA kit was certified to have indicated 100% sensitivity and 99.5% specificity for the patients' positive samples (n = 520). The cutoff value for the diagnosis of hHCV was decided following the protocol of the test. The positive sample was serially diluted (ten times of two-fold dilution) using the sample diluent included in the kit for the standard curve of the anti-HCV antibody ELISA test. The standard sample, including positive and negative samples, was stored in the incubator for 1 h at room temperature. After the washing steps with the ELISA kit's buffer, HRP-conjugated secondary antibodies were incubated for 30 min at room temperature. The quantity of anti-HCV antibody was determined by 30 min of TMB reaction with hydrogen peroxide solution from Sigma-Aldrich. Using an ELISA reader (Versamax, Molecular Devices, USA), the OD was measured at a wavelength of 450 nm following quenching with a 1 : 1 volume ratio of 2 M sulfuric acid solution. After the quenching process, the solution was dropped on the electrode wells to perform the redox cycling measurement as described above. The redox cycling current difference between the TMB stock solution (OD = 0, without ox-TMB-2 molecules) and the diluted TMB solutions was set as a redox cycling signal for the ELISA kit.[31,32] The test results were also compared with the commercially available rapid test (lateral flow immunoassay) from Abbott Korea (Seoul, Korea) for the medical diagnosis of hHCV. The manufacturer provided that the sensitivity and specificity of this rapid test kit were certified to be 99.3% and 98.1%, respectively.

2.6 Computer simulation

The properties of VPE were simulated using COMSOL Multiphysics® software.[1,2] For the simulations, the electrodes were replicated using a two-dimensional rotation model. The model electrodes were designed as VPEs. The dielectric layer was placed between the two electrodes, corresponding to the generator and collector electrodes. In the model electrodes, two parameters were controlled: (1) electrode gap (10–700 nm) and (2) number of paired electrodes (from 1- to 10-pairs). The reference potential of the electrode cell was set as +197 mV, which is equal to the Ag/AgCl reference electrode, and the potential sweep range for the generator was −200 mV to +500 mV *versus* the reference potential. The stationary potential of the collector was set as −200 mV and +400 mV. The electrochemical reaction was simulated based on the Butler–Volmer equation. For the simulation, the maximum element size was set to be 33.5 μm and the minimum element size was set to be 0.15 μm. The standard redox potential of TMB was set to be 200 mV, and the diffusion coefficient of TMB was 1.0×10^{-9} m^2 s^{-1} from previous works.[2,33] The electrolyte's diffusion coefficient (D) was set as 1.0×10^{-9} m^2 s^{-1}.[2,33] The current signal of the simulated redox cycling was set as the difference between the reductive peak current and the oxidative peak current.

3. Results and discussion

3.1 Properties of VPE based on PEDOT:PSS

The redox cycling was used to amplify the amperometric signal through the repeated redox reactions for each analyte molecule. For the hypersensitive redox cycling, the number of electrode pairs was reported to be increased, and the electrode gap needs to be fabricated as narrow as possible because the transport of the analyte to the electrode was carried out by diffusion.[34–36] The practical approach to improve the sensitivity of redox cycling was proposed to make VPEs, as shown in Fig. 1(a). The VPE could be fabricated by repeated deposition of electrodes and dielectric layers, and then the electrodes could be exposed by the etching process, as shown in Fig. 1(b). As the deposition of metal and dielectric layer with the thickness of less than one micrometer could be easily possible, the electrode gap of VPE could be controlled to be on the submicrometer level.[10] The previous report fabricated VPE with metal electrodes and parylene-C as a dielectric material.[10] The etching was performed to expose the electrodes using multi-step fabrication processes, which required wet-etching processes for metal electrodes and dry-etching processes for the dielectric layer of parylene-C. As the fabrication was performed using multi-step fabrication processes, it took a long processing time and a low fabrication yield. Furthermore, the wet-etching process of the metal electrodes frequently resulted in the over-etching and contamination of neighboring electrodes.[11,12] Using PEDOT:PSS as an electrode material for VPE, the problems of the metal electrode could be overcome, and the etching process could be carried out as a single step using RIE under the condition of O_2 and CF_4.[9] The thickness of the parylene defines the electrode gap between the electrodes, and the VPEs with multiple pairs of PEDOT:PSS electrodes are effectively fabricated for multiple paired electrodes.[2] The contamination and the over-etching problems from the repeated wet-etching process could also be overcome using a single-step RIE-etching. Using the RIE-etching, the parylene-C film could also be etched together with the PEDOT:PSS electrode, and the thickness of parylene can be controlled on the nanometer scale.[9,21] As shown in Fig. 1(c), the SEM images show that VPEs with 1-, 2- and 3-pair electrodes were fabricated using PEDOT:PSS as an electrode material, and the electrode pairs within VPE are clearly exposed after the RIE-etching process.

The conducting polymer, PEDOT:PSS, is usually reported to have properties of metal electrodes at strongly acidic conditions because the interaction between PEDOT and PSS is changed.[37,38] As shown in Fig. 2(a), polystyrene sulfonate (PSS^-) is known to be reduced to polystyrene sulfonic acid (PSSH), and hydrogen sulfate (HSO_4^-) has a coulombic interaction with PEDOT after the treatment of sulfuric acid. Such a reaction is known to change the conformation of PEDOT:PSS

 This journal is © The Royal Society of Chemistry 2023

Published on 21 febbraio 2023. Downloaded on 26/04/2026 03:20:33.

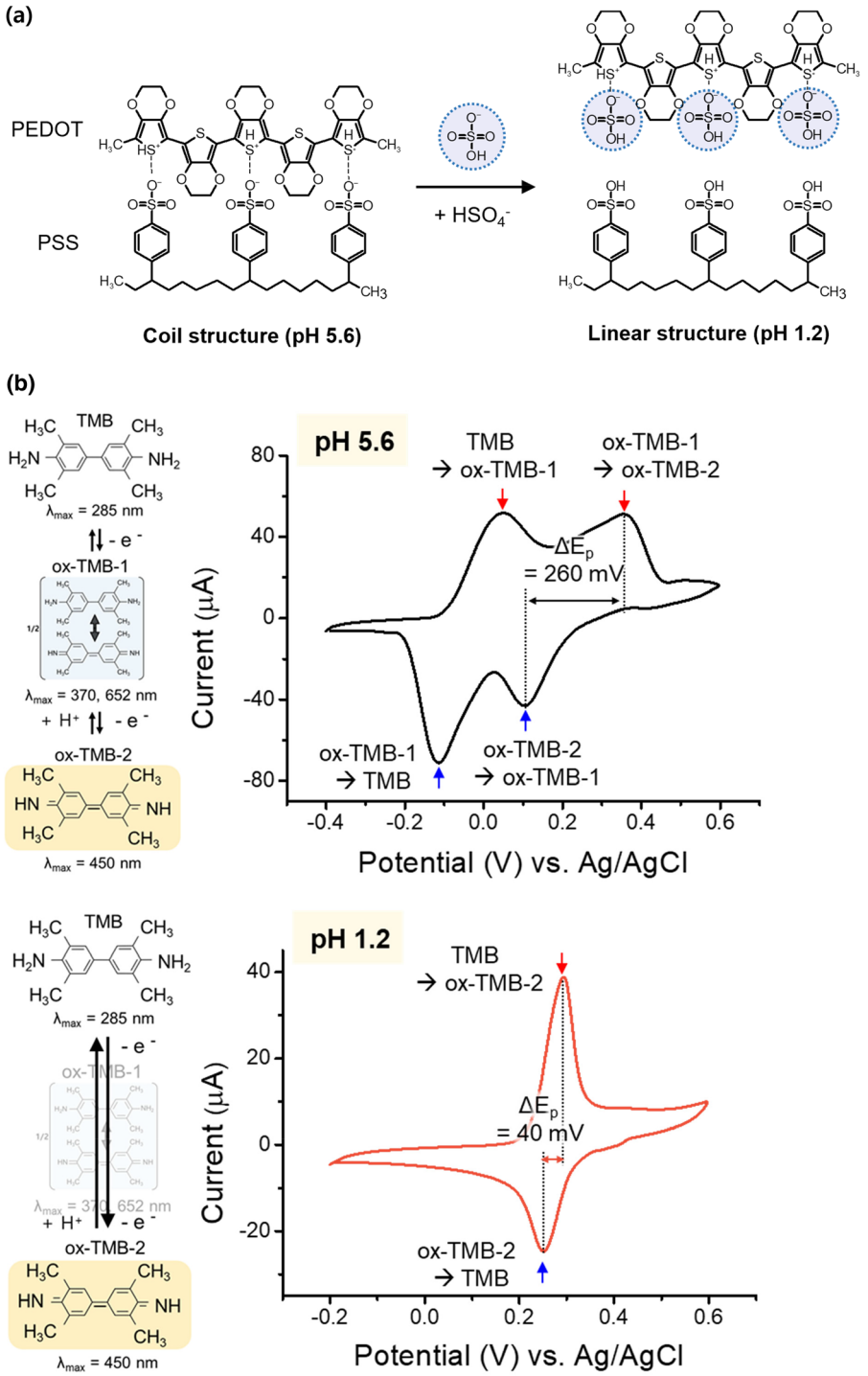

Fig. 2 Electrochemical properties of PEDOT:PSS. (a) Structure of PEDOT:PSS at different pH values. (b) CV analysis of TMB at different pH conditions using the PEDOT:PSS electrode. (c) Conductivity and apparent electron transfer rate of PEDOT:PSS at different pH conditions. Inset presents the cyclic voltammogram of 50 mM ferricyanide + 1 M KCl for k_{app} estimation. (d) Double-layer capacitance of the PEDOT:PSS electrode at different pH conditions.

from the coiled structure to the linear structure, reducing the energy barrier and improving the electron transfer. This work applied PEDOT:PSS as an electrode for VPE. Because the commercial immunoassays have frequently used the chromogenic reaction between an enzyme called HRP and TMB as a chromogenic substrate, the feasibility of PEDOT:PSS for the amperometric analysis of TMB was estimated. From the enzyme (HRP) reaction in immunoassays, TMB is oxidized through two step

Published on 21 febbraio 2023. Downloaded on 26/04/2026 03:20:33.

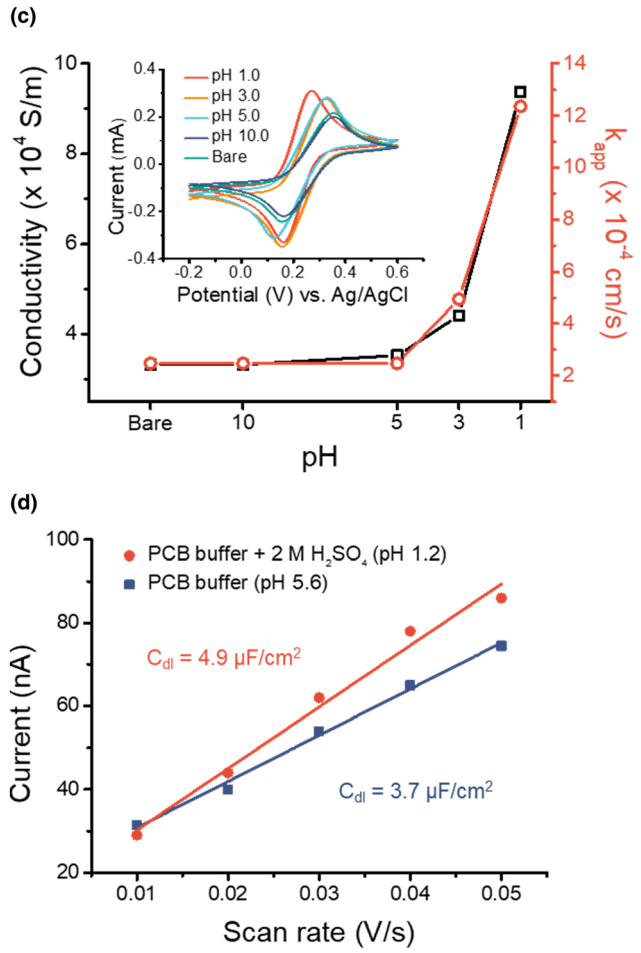

Fig. 2 *(Contd)*.

oxidation reaction:[1,33] TMB (λ_{max} = 285 nm, transparent) → ox-TMB-1 (λ_{max} = 652, 370 nm, blue color, pH = 5.6) → ox-TMB-2 (λ_{max} = 450 nm, yellow color, pH = 1.2).[7,39,40] At strongly acidic condition, the equilibrium between ox-TMB-1 and ox-TMB-2 was directed predominantly to the production of ox-TMB-2.[7,41] At first, the redox reaction of TMB at such different pH conditions was analyzed using the PEDOT:PSS electrode. As shown in Fig. 2(b), both oxidized TMB products (ox-TMB-1 and ox-TMB-2) could be observed at pH 5.6 using cyclic voltammetry (CV) with a working electrode (made of PEDOT:PSS with an electrode area of 27 mm^2).[1,42] After treatment of 2 M sulfuric acid (at pH 1.2), the ox-TMB-1 product was rapidly changed into ox-TMB-2, and the ox-TMB-1 peak disappeared in the cyclic voltammogram. When the shapes of the cyclic voltammograms at two different pH conditions were compared, the peak potential separation (ΔE_p) was changed from 260 mV (pH 5.6) to 40 mV (pH 1.2) at acidic pH. These results showed that the reversibility of the redox reaction for TMB could be significantly improved at pH 1.2 when PEDOT:PSS was used as a working electrode for CV.[37,43,44]

For the analysis of influencing factors for the electrochemical properties of PEDOT:PSS, the change in conductivity (σ), electron transfer rate constant (k_{app}), and double-layer capacitance (C_{dl}) were estimated at different pH conditions. When the conductivity was estimated using a four-point probe measurement (KEITHLEY 2400 source meter, USA) at different pH conditions, the conductivity was observed to be steeply increased from 3.3 × 10^4 S m^{-1} (pH 10.0) to 9.4 × 10^4 S m^{-1} (pH 1.0), as shown in Fig. 2(c). These results indicated that the PEDOT:PSS changed to have the property of a conductive electrode (Au: 4.1 × 10^7 S m^{-1}, Pt: 9.4 × 10^6 S m^{-1}, glassy carbon: 2.2 × 10^4 S m^{-1}, graphite: 2.1 × 10^3 S m^{-1})[45–47] at strongly acidic condition.[37,38] Additionally, the peak potential separation ($\Delta E_p = E_{ap} - E_{cp}$) between the cathodic and anodic peaks of CV was observed to be decreased at strongly acidic condition from the comparison of the cyclic voltammograms of TMB. Such change in the peak potential separation represented the improved reversibility of the redox reaction, which was correlated to the increase of the apparent electron transfer rate constant (k_{app}).[27,28] From the CV analysis, the apparent electron transfer rate constant (k_{app}) was 6.2 × 10^{-2} cm s^{-1} for PEDOT:PSS. These results also indicated that the PEDOT:PSS changed to have the property of a metal electrode (Au: 0.1 cm s^{-1}, Pt: 0.2 cm s^{-1}, glassy carbon: 6.6 × 10^{-3} cm s^{-1}, graphite: 10^{-6} cm s^{-1})[7] with a significantly increased conductivity at strongly acidic condition.[37,38] Therefore, PEDOT:PSS was observed to have improved conductivity and CV parameters at strongly acidic condition, which was used for the immunoassays based on the enzyme reaction of HRP and TMB. The double-layer capacitance of PEDOT:PSS was also calculated at different pH conditions. From the CV analysis, the PEDOT:PSS electrode had a double-layer capacitance of 3.7 μF cm^{-2} at pH 5.6 and 4.9 μF cm^{-2} at pH 1.2, as shown in Fig. 2(d). The PEDOT:PSS electrode was estimated to have a far lower double-layer capacitance than the conventional metal electrodes,[5] which indicated that the lower *i–V* background in CV analysis could be achieved in comparison with the conventional metal electrodes.[48,49] These results showed that the PEDOT:PSS electrode's properties were changed to be near the metal electrodes, such as a high electron transfer rate and a high conductivity. From these results, the conducting polymer, PEDOT:PSS, was chosen as an optimal electrode material for the analysis of TMB at the strongly acidic pH, which had been used for the immunoassays based on the enzyme reaction of HRP and TMB.[23,50] The electrochemical parameters are summarized in Table 1 in comparison with other electrode materials, such as carbon electrodes and metal electrodes.

Table 1 Characterization of the electrochemical properties of electrode materials

	Conductivity (S m^{-1})	ΔE_p (mV)	k_{app} (cm s^{-1})	C_{dl} (μF cm^{-2})	Ref.
PEDOT:PSS (at pH 1.2)	9.4 × 10^4	40	6.2 × 10^{-2}	4.9	This work
Gold	4.1 × 10^7	80	0.1	30.9	7 and 45
Pt	9.4 × 10^6	70	0.2	64.2	7 and 45
Glassy carbon	2.2 × 10^4	60	6.6 × 10^{-3}	12.9	7 and 47
Graphite	2.1 × 10^3	60	10^{-6}	5.0	7 and 46

This journal is © The Royal Society of Chemistry 2023

Published on 21 febbraio 2023. Downloaded on 26/04/2026 03:20:33.

3.2 Redox cycling of TMB with VPE

The VPE fabricated with PEDOT:PSS as an electrode material and parylene for dielectric layers was used for the redox cycling of ox-TMB-2 using the generator electrode and collector electrode.[1,2] The potential of the collector electrode for redox cycling was determined from CV analysis of TMB. As shown in Fig. 2(b), the anodic peak for the oxidation of TMB (TMB to ox-TMB-2) was observed at the potential of 290 mV against the Ag/AgCl reference electrode, and the cathodic peak for reduction of TMB (ox-TMB-2 to TMB) was observed at the potential of 250 mV against the Ag/AgCl reference electrode.[7,51] The redox cycling was carried out by changing the potential of the collector electrode while the CV was performed at the generator electrode, as shown in Fig. 3(a). As the first step, the potential of the collector electrode was set at a reductive potential of −200 mV against the Ag/AgCl electrode while the generator electrode carried out the CV of ox-TMB-2. The fixed potential of the collector electrode at −200 mV was used for the reduction of ox-TMB-2 (into TMB), which amplified the oxidative current of the cyclic voltammogram at the generator electrode (noted as "(1)"). As the second step, the potential of the collector electrode was set to an oxidative potential of +400 mV against the Ag/AgCl electrode while the generator

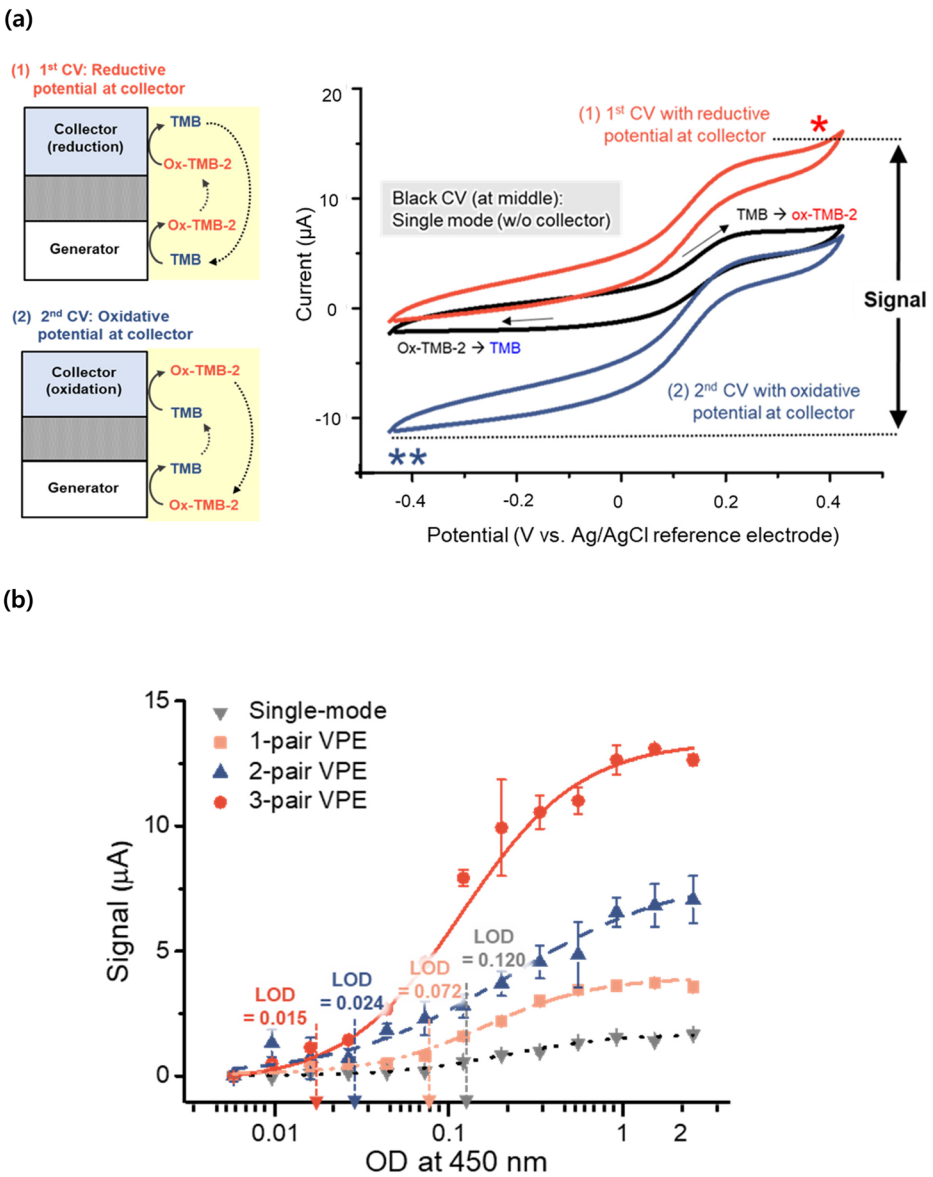

Fig. 3 Redox cycling of TMB using the vertically paired electrode (VPE). (a) Redox cycling of TMB using the alternating potential of the collector electrode. (b) Standard curve for the redox cycling of ox-TMB-2 at different pairs of electrodes. (c) Comparison of the simulation and experimental data of the redox cycling signal for different electrode gaps. (d) Comparison of the simulated and experimental data of the redox cycling signal for different electrode pairs.

Published on 21 febbraio 2023. Downloaded on 26/04/2026 03:20:33.

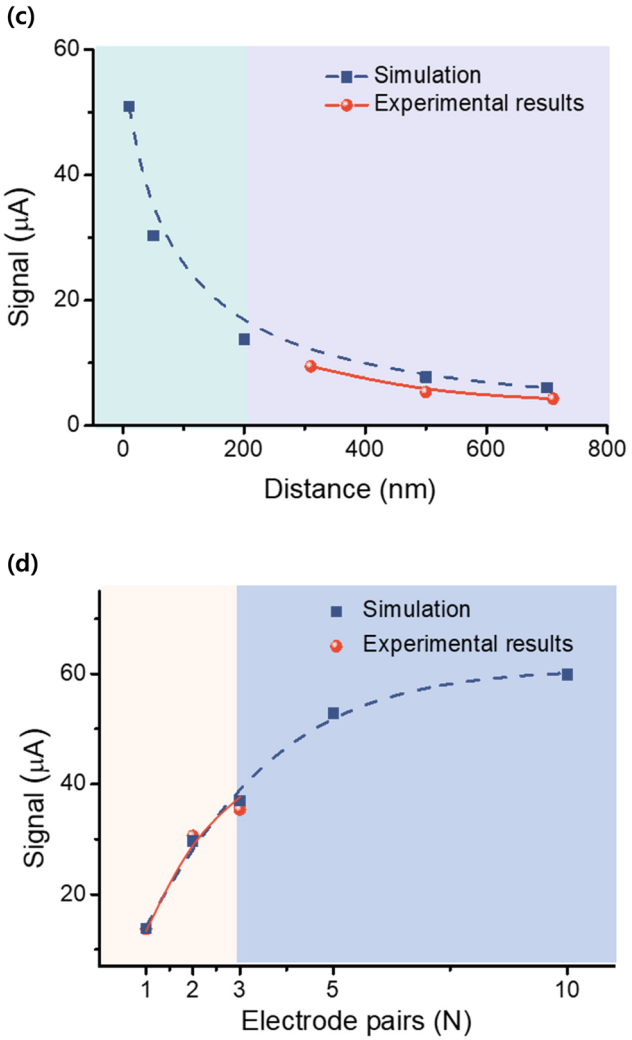

Fig. 3 *(Contd)*.

electrode carried out the CV of ox-TMB-2. The fixed potential of the collector electrode at +400 mV was used for the oxidation of TMB (into ox-TMB-2), which amplified the reductive current of the cyclic voltammogram at the generator electrode (noted as "(2)"). The final signal was calculated from the difference between the increased reductive current of the first step (noted as "*") and the increased oxidative current at the second step (noted as "**").[1,2]

The redox cycling was performed for standard TMB solutions at different OD values. The standard samples were made by diluting the ox-TMB-2 solution after quenching with 2 M sulfuric acid. As shown in Fig. 3(b), the redox cycling of the standard TMB solution was carried out using 1-pair, 2-pair, and 3-pair VPEs with a fixed electrode gap of 500 nm. When the results were compared with the conventional single-mode electrode, the detection range of 3-pair VPE, as well as the limit of detection (LOD) of VPE, appeared to be far improved in comparison with the single-mode measurement with the LOD of 0.015 (in OD unit). The measurement sensitivity was observed to increase as the number of electrode pairs increased for VPE. When the amplification ratio of redox cycling was estimated for the TMB sample at the OD value of 1.0, the redox cycling signal apparently reached the saturation for the 3-paired VPE. When the redox cycling signal at the OD value of 1.0 was compared with the single-mode amperometry (1.6 μA), the redox cycling signal was estimated to be amplified as high as 3.6 μA (2.3-fold amplification) for the 1-pair VPE, 6.6 μA (4.2-fold amplification) for the 2-pair VPE, and 12.7 μA (8.2-fold amplification) for the 3-pair VPE in comparison with the single-mode amperometry. Such an increased sensitivity was considered to occur from the influencing factors for the redox cycling based on VPE, such as the number of electrode pairs and the electrode gap. Although the electrode pair above the five were difficult to fabricate in this study, the VPEs could realize a very sensitive immunoassay with redox cycling detection.

The properties of VPE were simulated using COMSOL Multiphysics® software.[1,2] For the simulations, the electrodes were replicated using a two-dimensional rotation model, as shown in Fig. S2(a).† Through the computer simulation, VPEs were designed to have a narrow electrode gap and a high number of electrode pairs, which were limited to fabricate using a lab-based fabrication process. The electrode model was designed for VPE using the electrical conductivity (σ) and dielectric constant (ε) of the PEDOT:PSS and parylene film, as shown in Fig. S2(a).†[33,52,53] In order to estimate the influence of the electrode gap on the redox cycling signal, VPEs (1-pair) were fabricated with the controlled electrode gaps of 700 nm, 500 nm, and 300 nm. As shown in Fig. 3(c), these VPEs were used for the redox cycling of TMB (Fig. S2(b)†), and the redox cycling signal was measured to be 4.28 μA, 5.4 μA, and 9.4 μA for VPE with the electrode gap of 700 nm, 500 nm, and 300 nm, respectively. VPEs with the controlled electrode gaps of 200 nm, 50 nm and 10 nm were then designed for computer simulation, and the redox cycling signal was calculated to be increased to be 6.0 μA, 7.7 μA, 13.8 μA, 30.4 μA and 51.0 μA for VPE with the electrode gap of 700 nm, 500 nm, 200 nm, 50 nm and 10 nm, respectively. These results from the real experiment and computer simulation showed that a steep increase could be made as the electrode gap decreased to less than 100 nm. The influence of number of electrode pairs was estimated by fabricating 1-, 2- and 3-pair VPEs (with an electrode gap of 500 nm). As shown in Fig. 3(d), these VPEs were used for the redox cycling of TMB (Fig. S2(c)†), and the redox cycling signal was measured to be 15.6 μA, 36.2 μA and 39.9 μA for 1-, 2- and 3-pair VPEs, respectively. VPEs with a large number of electrode pairs were then designed for computer simulation, and the redox cycling signal was calculated to increase to 13.8 μA, 29.7 μA, 37.0 μA, 52.9 μA and 59.9 μA for the 1-, 2-, 3-, 5- and 10-pair VPEs, respectively. These results from the real experiment and computer simulation showed that a steep increase of the redox cycling signal could be made as the electrode gap decreased to be less than 100 nm, and the number of electrodes in VPEs increased to be larger than 5-pairs using the improved fabrication method.

This journal is © The Royal Society of Chemistry 2023

Published on 21 febbraio 2023. Downloaded on 26/04/2026 03:20:33.

3.3 Application of redox cycling to immunoassays

Amperometric measurements for immunoassays have been reported in previous works because of the advantages of electrochemical methods, such as simple instrumentation and high sensitivity.[7,13,14,32] In this work, the hypersensitive electrochemical analysis of the immunoassay was demonstrated for the quantification of ox-TMB-2 using the redox cycling with vertically paired electrode (VPE). As shown in Fig. 4(a), ELISA tests consist of sequential treatment of anti-HCV antibodies and secondary antibodies conjugated with HRP. The immunoassay aimed to quantify the target analytes (hHCV antibody) using the enzyme reaction of HRP, and TMB was used as a chromogenic substrate. After the fixed reaction time (30 min), the enzyme (HRP) reaction was quenched with 2 M sulfuric acid and the ox-TMB-1 was further oxidized into ox-TMB-2 (λ_{max} = 450 nm). This immunoassay was carried out according to the manufacturer's instruction. The redox cycling was then carried out for the quantification of ox-TMB-2.[1,2]

For the application of the redox cycling method to the ELISA test, the VPEs with different numbers of electrode pairs were used for the commercial hHCV ELISA test. The redox cycling with the VPE (with an electrode gap of 500 nm) was applied to the immunoassay for the detection of hHCV antibodies. The redox cycling signal was measured by changing the potential of the collector electrode (at the oxidative potential of +400 mV and at the reductive potential of −100 mV *vs.* the Ag/AgCl reference electrode). The standard hHCV samples were prepared by serial dilution of positive sera in the ELISA kit. For comparison, chromogenic detection at 450 nm was measured for the same reaction solution. For both analysis methods, the three standard deviations and the mean value of the negative sample were used to calculate the LOD. The cutoff value for the medical diagnosis of hHCV was estimated using

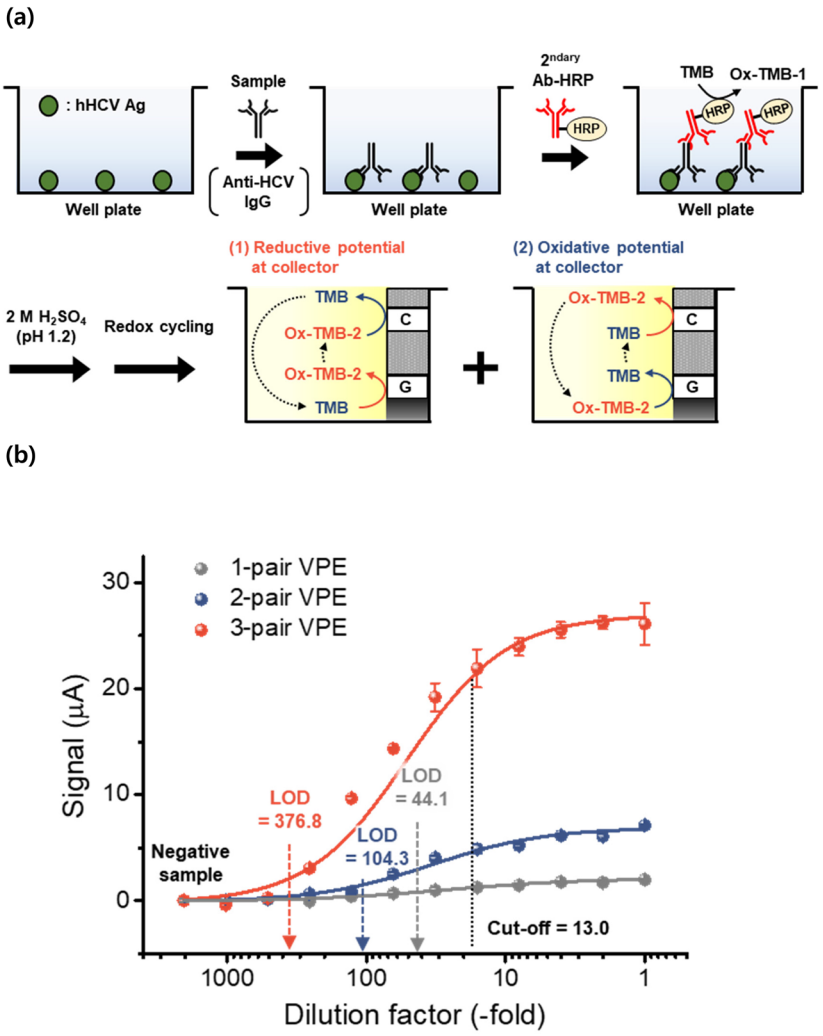

Fig. 4 Immunoassay of the anti-HCV antibody with vertically paired electrodes. (a) Schematic view of the immunoassay procedure for the anti-HCV antibody. (b) Comparison of sensitivities for the anti-HCV antibody ELISA kit according to the number of electrode pairs. (c) Standard curve for detecting anti-HCV antibodies using redox cycling with the 3-pair VPE, chemiluminescence assay, and chromogenic method. (d) Comparison of assay results between the 3-pair VPE redox cycling and the rapid test (lateral flow immunoassay).

Published on 21 febbraio 2023. Downloaded on 26/04/2026 03:20:33.

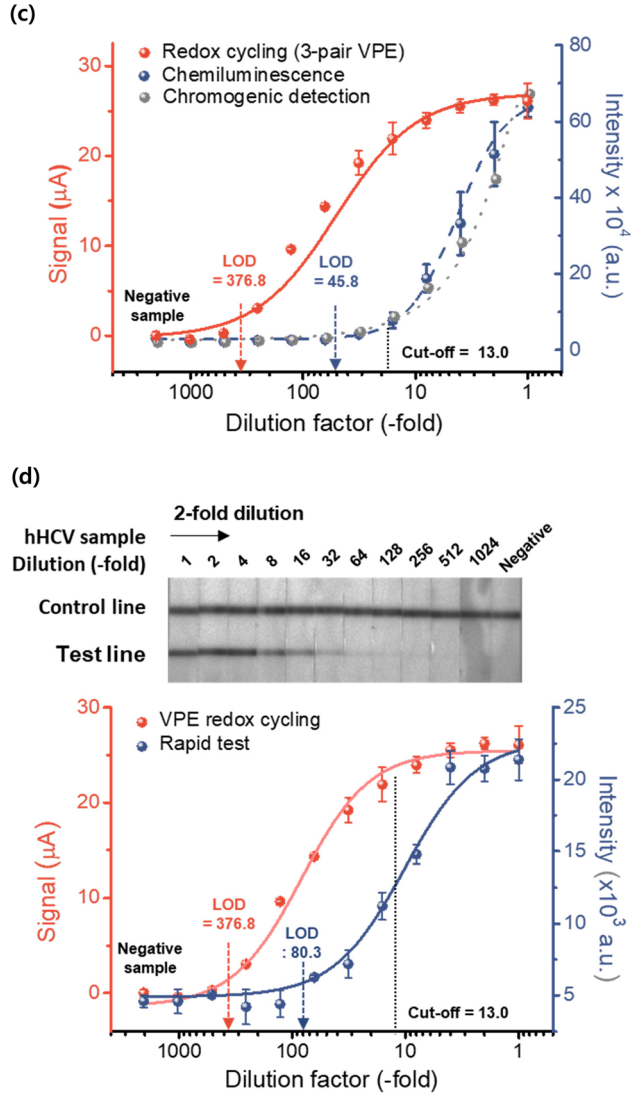

Fig. 4 *(Contd).*

instructions from the manufacturer of the ELISA kit (cutoff value = 0.1 plus OD for the negative control at the wavelength of 450 nm). When the VPE with different number of electrode pairs was used for redox cycling, the sensitivity of redox cycling was observed to increase with increasing number of electrode pairs in VPE. As shown in Fig. 4(b), the 3-pair VPE showed the highest signal among the three kinds of VPEs in the whole concentration range. The LOD was estimated to be for 44.1 (unit of dilution factor) for 1-pair VPE, 104.3 for 2-pair VPE and 376.8 for 3-pair VPE. These results showed that the redox cycling-based VPE with 3-pair electrodes could have more than 8-fold increased sensitivity in comparison with VPE with 1-pair electrode.

The sensitivity of the redox cycling method was compared with the conventional detection methods based on chromogenic reaction and luminol-based chemiluminescence.[15,16] The standard hHCV samples were also prepared by serial dilution of positive sera in the ELISA kit. As shown in Fig. 4(c), the LOD was estimated to be for 13.0 (unit of dilution factor) for the chromogenic reaction, 45.8 for chemiluminescence and 376.8 for redox cycling with 3-pair VPE. These results indicate that the redox cycling based on the 3-pair electrode had a far higher sensitivity and a wider detection range than the conventional methods based on the chromogenic reaction and luminol-based chemiluminescence. The assay results for the hHCV ELISA test based on redox cycling was also compared with a commercially available rapid test (lateral flow immunoassay) for the diagnostics of hHCV. The standard hHCV samples were also prepared by serial dilution of positive sera in the ELISA kit. As shown in Fig. 4(d), the LOD value was calculated to be 80.3 (unit of dilution factor) for the rapid test kit and 376.8 for the redox cycling with VPE. These results showed that the redox cycling with VPE could be used to diagnose hHCV with a far higher sensitivity and a wider detection range compared with the rapid test.

4. Conclusions

An electrochemical immunoassay based on the redox cycling method was presented using vertically paired electrodes (VPEs), which were fabricated using poly(3,4-ethylenedioxythiophene):poly(styrenesulfonate) (PEDOT:PSS) as an electrode material and parylene-C as a dielectric layer. For the application to immunoassays, different electrochemical properties of PEDOT:PSS were analyzed for the redox reaction of 3,3′,5,5′-tetramethylbenzidine (TMB, the chromogenic substrate for immunoassays) at different pH conditions, such as conductivity (σ), electron transfer rate constant (k_{app}), and double-layer capacitance (C_{dl}). The PEDOT:PSS in acidic conditions exhibited an electron transfer rate constant similar to that of metal electrodes, but much faster than that of carbon electrodes. The double-layer capacitance was similar to that of carbon electrodes, which had a far lower *I–V* background, so CV analysis could be achieved in comparison with the conventional metal electrodes. The influencing factors on the sensitivity of redox cycling with VPEs based on PEDOT:PSS were analyzed for the redox reaction of TMB, such as the electrode gap and number of electrode pairs. In this study, two parameters of the electrode were controlled: (1) the electrode gaps (300 nm, 500 nm, 700 nm) by controlling the thickness of the parylene film, and (2) the number of electrodes (1-pair, 2-pair, 3-pair). The effect of the electrode gap and the number of electrodes on the redox cycling measurement were analyzed with vertically paired electrodes. The sensitivity of the redox cycling measurement in TMB was observed to increase with a decrease in the electrode gap and an increase in the number of electrodes. Computer simulation was also performed for the redox cycling results based on VPEs, which had limitations in fabrication, such as VPEs with an electrode gap of less than 100 nm and more than five electrode pairs. Finally, the redox cycling based on VPE was applied to the commercial ELISA kit test to detect the human hepatitis-C virus (hHCV) antibodies. The vertically paired electrode-based redox cycling measurement

This journal is © The Royal Society of Chemistry 2023

showed that more sensitive detection could be achieved in comparison with conventional detection methods, such as chromogenic detection, luminol-based chemiluminescent detection and the commercially available rapid test (lateral flow immunoassay).

Abbreviations

PEDOT	Poly(3,4-ethylenedioxythiophene)
PSS	Poly(styrenesulfonate)
TMB	3,3′,5,5′-Tetramethylbenzidine
hHCV	Human hepatitis-C virus
IDE	Interdigitated electrode
WE	Working electrode
VPE	Vertically paired electrode
RIE	Reactive-ion etching
HRP	Horseradish peroxidase
PR	Photoresist
CV	Cyclic voltammetry

Conflicts of interest

There are no conflicts to declare.

Acknowledgements

This work was supported by the National Research Foundation of Korea [NRF-2020R1A5A101913111 and NRF-2021R1A2C209370611].

References

1 G. Y. Lee, J. H. Park, Y. W. Chang, S. Cho, M. J. Kang and J. C. Pyun, Chronoamperometry-Based Redox Cycling for Application to Immunoassays, *ACS Sens.*, 2018, **3**, 106–112.
2 G. Y. Lee, J. H. Park, Y. W. Chang, S. Cho, M. J. Kang and J. C. Pyun, Redox cycling-based immunoassay for detection of carcinogenic embryonic antigen, *Anal. Chim. Acta*, 2017, **971**, 33–39.
3 M. Huske, R. Stockmann, A. Offenhausser and B. Wolfrum, Redox cycling in nanoporous electrochemical devices, *Nanoscale*, 2014, **6**, 589–598.
4 B. Wolfrum, E. Katelhon, A. Yakushenko, K. J. Krause, N. Adly, M. Huske and P. Rinklin, Nanoscale Electrochemical Sensor Arrays: Redox Cycling Amplification in Dual-Electrode Systems, *Acc. Chem. Res.*, 2016, **49**, 2031–2040.
5 O. Niwa, M. Morita and H. Tabei, Fabrication and Characteristics of Vertically Separated Interdigitated Array Electrodes, *J. Electroanal. Chem.*, 1989, **267**, 291–297.
6 O. Niwa, M. Morita and H. Tabei, Electrochemical-Behavior of Reversible Redox Species at Interdigitated Array Electrodes with Different Geometries – Consideration of Redox Cycling and Collection Efficiency, *Anal. Chem.*, 1990, **62**, 447–452.
7 J. H. Park, Z. Song, G. Y. Lee, S. M. Jeong, M. J. Kang and J. C. Pyun, Hypersensitive electrochemical immunoassays based on highly N-doped silicon carbide (SiC) electrode, *Anal. Chim. Acta*, 2019, **1073**, 30–38.
8 J. M. Guerrero, F. S. Aguirre, M. L. Mota and A. Carrillo, Advances for the Development of In Vitro Immunosensors for Multiple Sclerosis Diagnosis, *BioChip J.*, 2021, **15**, 205–215.
9 J. H. Park, G. Y. Lee, Z. Song, J. H. Bong, Y. W. Chang, S. Cho, M. J. Kang and J. C. Pyun, Capacitive biosensor based on vertically paired electrodes for the detection of SARS-CoV-2, *Biosens. Bioelectron.*, 2022, **202**, 113975.
10 G. Y. Lee, J. H. Park, Y. W. Chang, M. J. Kang, S. Cho and J. C. Pyun, Capacitive biosensor based on vertically paired electrode with controlled parasitic capacitance, *Sens. Actuators, B*, 2018, **273**, 384–392.
11 C. J. Brennan, C. M. Neumann and S. A. Vitale, Comparison of gate dielectric plasma damage from plasma-enhanced atomic layer deposited and magnetron sputtered TiN metal gates, *J. Appl. Phys.*, 2015, **118**, 045307.
12 H. Takeuchi, M. She, K. Watanabe and T. J. King, Damageless sputter depositions by plasma charge trap for metal gate technologies, *IEEE Trans. Semiconduct. Manuf.*, 2005, **18**, 350–354.
13 P. Fanjul-Bolado, M. B. Gonzalez-Garcia and A. Costa-Garcia, Amperometric detection in TMB/HRP-based assays, *Anal. Bioanal. Chem.*, 2005, **382**, 297–302.
14 G. Volpe, R. Draisci, G. Palleschi and D. Compagnone, 3,3′,5,5′-Tetramethylbenzidine as electrochemical substrate for horseradish peroxidase based enzyme immunoassays. A comparative study, *Analyst*, 1998, **123**, 1303–1307.
15 H. R. Kim, J. H. Bong, J. H. Park, Z. Song, M. J. Kang, D. H. Son and J. C. Pyun, Cesium Lead Bromide ($CsPbBr_3$) Perovskite Quantum Dot-Based Photosensor for Chemiluminescence Immunoassays, *ACS Appl. Mater. Interfaces*, 2021, **13**, 29392–29405.
16 K. Takeda, M. Maruki, T. Yamagaito, M. Muramatsu, Y. Sakai, H. Tobimatsu, H. Kobayashi, Y. Mizuno and Y. Hamaguchi, Highly sensitive detection of hepatitis B virus surface antigen by use of a semiautomated immune complex transfer chemiluminescence enzyme immunoassay, *J. Clin. Microbiol.*, 2013, **51**, 2238–2244.
17 N. L. Gao, J. G. Chang, Z. M. Zhu and H. You, Multistory Stairs-based, Fast and Point-of-care Testing for Disease Biomarker Using One-step Capillary Microfluidic Fluoroimmunoassay Chip via Continuous On-chip Labelling, *BioChip J.*, 2021, **15**, 268–275.
18 S. K. Kim, H. Sung, S. H. Hwang and M. N. Kim, A New Quantum Dot-Based Lateral Flow Immunoassay for the Rapid Detection of Influenza Viruses, *BioChip J.*, 2022, **16**, 175–182.
19 G. Y. Lee, Y. H. Choi, H. W. Chung, H. Ko, S. Cho and J. C. Pyun, Capacitive immunoaffinity biosensor based on

Published on 21 febbraio 2023. Downloaded on 26/04/2026 03:20:33.

Published on 21 febbraio 2023. Downloaded on 26/04/2026 03:20:33.

vertically paired ring-electrodes, *Biosens. Bioelectron.*, 2013, **40**, 227–232.
20 Y. Lim, J.-I. Heo and H. Shin, Fabrication and application of a stacked carbon electrode set including a suspended mesh made of nanowires and a substrate-bound planar electrode toward for an electrochemical/biosensor platform, *Sens. Actuators, B*, 2014, **192**, 796–803.
21 Z. Song, J. H. Im, H. Ko, J. H. Park, G. Y. Lee, M. J. Kang, M. H. Kim and J. C. Pyun, Plasma deposition of parylene-C film, *Mater. Today Commun.*, 2021, **26**, 101834.
22 J. H. Park, Z. Song, J. H. Bong, H. R. Kim, M. J. Kim, K. H. Choi, S. S. Shin, M. J. Kang, D. Y. Lee and J. C. Pyun, Electrochemical One-Step Immunoassay Based on Switching Peptides and Pyrolyzed Carbon Electrodes, *ACS Sens.*, 2022, **7**, 215–224.
23 P. Tehrani, A. Kanciurzewska, X. Crispin, N. Robinson, M. Fahlman and M. Berggren, The effect of pH on the electrochemical over-oxidation in PEDOT:PSS films, *Solid State Ionics*, 2007, **177**, 3521–3527.
24 B. H. Suryanto, S. Chen, J. Duan and C. Zhao, Hydrothermally Driven Transformation of Oxygen Functional Groups at Multiwall Carbon Nanotubes for Improved Electrocatalytic Applications, *ACS Appl. Mater. Interfaces*, 2016, **8**, 35513–35522.
25 A. Q. Mugheri, A. Tahira, U. Aftab, M. I. Abro, S. R. Chaudhry, L. Amaral and Z. H. Ibupoto, Facile efficient earth abundant NiO/C composite electrocatalyst for the oxygen evolution reaction, *RSC Adv.*, 2019, **9**, 5701–5710.
26 T. Tichter, J. Schneider and C. Roth, Finite Heterogeneous Rate Constants for the Electrochemical Oxidation of VO^{2+} at Glassy Carbon Electrodes, *Front. Energy Res.*, 2020, **8**, 155.
27 R. S. Nicholson, Theory and Application of Cyclic Voltammetry for Measurement of Electrode Reaction Kinetics, *Anal. Chem.*, 2002, **37**, 1351–1355.
28 H. Muhammad, I. A. Tahiri, M. Muhammad, Z. Masood, M. A. Versiani, O. Khaliq, M. Latif and M. Hanif, A comprehensive heterogeneous electron transfer rate constant evaluation of dissolved oxygen in DMSO at glassy carbon electrode measured by different electrochemical methods, *J. Electroanal. Chem.*, 2016, **775**, 157–162.
29 J. Zhou, K. Ren, Y. Zheng, J. Su, Y. Zhao, D. Ryan and H. Wu, Fabrication of a microfluidic Ag/AgCl reference electrode and its application for portable and disposable electrochemical microchips, *Electrophoresis*, 2010, **31**, 3083–3089.
30 S. Maity, S. Nandi, S. Biswas, S. K. Sadhukhan and M. K. Saha, Performance and diagnostic usefulness of commercially available enzyme linked immunosorbent assay and rapid kits for detection of HIV, HBV and HCV in India, *Virol. J.*, 2012, **9**, 290.
31 A. Crew, C. Alford, D. C. C. Cowell and J. P. Hart, Development of a novel electrochemical immuno-assay using a screen printed electrode for the determination of secretory immunoglobulin A in human sweat, *Electrochim. Acta*, 2007, **52**, 5232–5237.
32 J. K. Lee, G. Yoo, M. Park, J. Jose, M. J. Kang and J. C. Pyun, Electrochemical ELISA based on Escherichia coli with auto-displayed Z-domains, *Sens. Actuators, B*, 2012, **175**, 46–52.
33 G. Y. Lee, Y. W. Chang, H. Ko, M. J. Kang and J. C. Pyun, Band-type microelectrodes for amperometric immunoassays, *Anal. Chim. Acta*, 2016, **928**, 39–48.
34 A. Aggarwal, M. Hu and I. Fritsch, Detection of dopamine in the presence of excess ascorbic acid at physiological concentrations through redox cycling at an unmodified microelectrode array, *Anal. Bioanal. Chem.*, 2013, **405**, 3859–3869.
35 M. Hu and I. Fritsch, Application of Electrochemical Redox Cycling: Toward Differentiation of Dopamine and Norepinephrine, *Anal. Chem.*, 2016, **88**, 5574–5578.
36 T. Horiuchi, O. Niwa, M. Morita and H. Tabei, Limiting Current Enhancement by Self-Induced Redox Cycling on a Micro-Macro Twin Electrode, *J. Electrochem. Soc.*, 1991, **138**, 3549–3553.
37 Y. Xia, K. Sun and J. Ouyang, Solution-processed metallic conducting polymer films as transparent electrode of optoelectronic devices, *Adv. Mater.*, 2012, **24**, 2436–2440.
38 D. Xu, H. Shen, W. Wang, J. Xie, T. Zhang, H. Yuan, Y. Li, X. Chen, Y. He and Y. Zhang, Effect of H_2SO_4 Solution Treatment on Adhesion, Charge Transfer, and Catalytic Performance of Screen-Printed PEDOT:PSS, *ChemPhysChem*, 2019, **20**, 374–382.
39 J. I. Kim, A. Bordeanu and J. C. Pyun, Diamond-like carbon (DLC) microelectrode for electrochemical ELISA, *Biosens. Bioelectron.*, 2009, **24**, 1394–1398.
40 S. D. Kim, J. W. Chung, J. T. Kim, H. Krause and J. C. Pyun, Gold-film array-electrode for electrochemical ELISA, *Sens. Actuators, B*, 2005, **111–112**, 463–469.
41 Y. Ha and I. Kim, Recent Developments in Innovative Magnetic Nanoparticles-Based Immunoassays: From Improvement of Conventional Immunoassays to Diagnosis of COVID-19, *BioChip J.*, 2022, **16**, 351–365.
42 J. Lee, D. Sharma, Y. Lim and H. Shin, Redox cycling effect at microchannel-integrated sandwich electrodes consisting of a suspended mesh and a substrate-bound planar electrode, *Sens. Actuators, B*, 2018, **267**, 467–475.
43 E. Hosseini, V. Ozhukil Kollath and K. Karan, The key mechanism of conductivity in PEDOT:PSS thin films exposed by anomalous conduction behaviour upon solvent-doping and sulfuric acid post-treatment, *J. Mater. Chem. C*, 2020, **8**, 3982–3990.
44 K. Wijeratne, U. Ail, R. Brooke, M. Vagin, X. Liu, M. Fahlman and X. Crispin, Bulk electronic transport impacts on electron transfer at conducting polymer electrode-electrolyte interfaces, *Proc. Natl. Acad. Sci. U. S. A.*, 2018, **115**, 11899–11904.
45 I. H. Tavman, Preparation and Characterization of Conductive Polymer Nanocomposites Based on Ethylene–Vinylacetate Copolymer (EVA) Reinforced with Expanded and Unexpanded Graphite, *Adv. Mater. Res.*, 2015, **1114**, 92–99.
46 B. Marinho, M. Ghislandi, E. Tkalya, C. E. Koning and G. de With, Electrical conductivity of compacts of gra-

 This journal is © The Royal Society of Chemistry 2023

Published on 21 febbraio 2023. Downloaded on 26/04/2026 03:20:33.

phene, multi-wall carbon nanotubes, carbon black, and graphite powder, *Powder Technol.*, 2012, **221**, 351–358.

47 L. Ferrer-Argemi, A. Cisquella-Serra, M. Madou and J. Lee, Temperature-Dependent Electrical and Thermal Conductivity of Glassy Carbon Wires, *2018 17th IEEE Intersoc. Conf. Therm. Thermomech. Phenom. Electron. Syst*, 2018, pp. 1280–1288. DOI: 10.1109/ITHERM.2018.8419618.

48 M. Panizza and G. Cerisola, Application of diamond electrodes to electrochemical processes, *Electrochim. Acta*, 2005, **51**, 191–199.

49 T. Watanabe, T. K. Shimizu, Y. Tateyama, Y. Kim, M. Kawai and Y. Einaga, Giant electric double-layer capacitance of heavily boron-doped diamond electrode, *Diamond Relat. Mater.*, 2010, **19**, 772–777.

50 M. M. de Kok, M. Buechel, S. I. E. Vulto, P. van de Weijer, E. A. Meulenkamp, S. H. P. M. de Winter, A. J. G. Mank, H. J. M. Vorstenbosch, C. H. L. Weijtens and V. van Elsbergen, Modification of PEDOT:PSS as hole injection layer in polymer LEDs, *Phys. Status Solidi A*, 2004, **201**, 1342–1359.

51 J.-K. Lee, Y. Gu, M. Park, J. Jose and J.-C. Pyun, Electrochemical ELISA Based on E. Coli with Autodisplayed Z-Domains, *Procedia Eng.*, 2011, **25**, 944–947.

52 I. S. D. Santos-Neto, C. D. Carvalho, G. B. A. Filho, C. Andrade, G. C. O. Santos, A. K. Barros, J. Neto, V. L. P. Casas, L. M. R. Alencar, A. J. O. Lopes, F. C. Silva and F. S. M. Sinfronio, Interdigitated Electrode for Electrical Characterization of Commercial Pseudo-Binary Biodiesel-Diesel Blends, *Sensors*, 2021, **21**, 7288.

53 S. Sathya, S. Muruganand, N. Manikandan and K. Karuppasamy, Design of capacitance based on interdigitated electrode for BioMEMS sensor application, *Mater. Sci. Semicond. Process.*, 2019, **101**, 206–213.